Assessing a Microwave Imaging System for Brain Stroke Monitoring via High Fidelity Numerical Modelling

Assessing a Microwave Imaging System for Brain Stroke Monitoring via High Fidelity Numerical Modelling

D. O. Rodriguez-Duarte, *Student Member*, *IEEE*, J. A. Tobon Vasquez, *Member*, *IEEE*, R. Scapaticci, *Member*, *IEEE*, L. Crocco, *Senior Member*, *IEEE* and F. Vipiana, *Senior Member*, *IEEE*

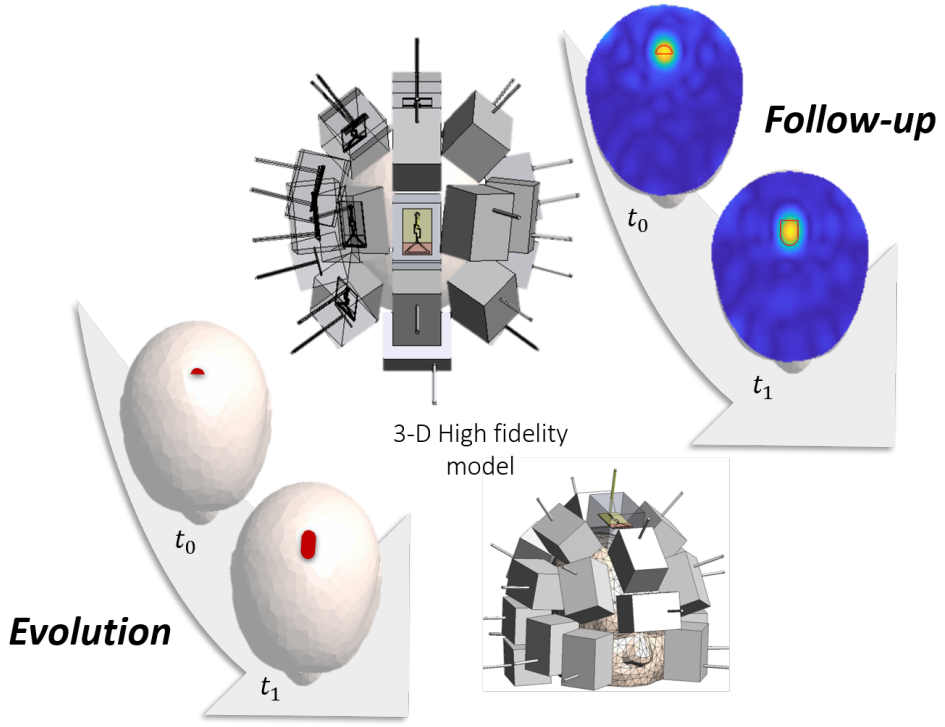

Brain Stroke Monitoring

Take-Home Messages

- This work deals with the use of microwave imaging (MWI) for brain stroke monitoring and presents a validation of an MWI prototype by means of a high-fidelity numerical model.
- The numerical analysis reported in the paper shows that the considered MWI system is capable of performing the monitoring of hemorrhages and clots.
- The paper deals with continuous monitoring of brain stroke, which is still an unmet clinical need which cannot be performed with currently adopted imaging modalities like magnetic resonance imaging (MRI) and computerized x-ray tomography (CT).
- The main claim of the work is to show how the adoption of a high-fidelity device-specific numerical model is important to perform in silico experiments of complex scenarios needed to address subsequent experimental activities.

Assessing a Microwave Imaging System for Brain Stroke Monitoring via High Fidelity Numerical Modelling

D. O. Rodriguez-Duarte, *Student Member, IEEE*, J. A. Tobon Vasquez, *Member, IEEE*, R. Scapaticci, *Member, IEEE*, L. Crocco, *Senior Member, IEEE* and F. Vipiana, *Senior Member, IEEE*

***Abstract*—This work presents the outcomes of a numerical analysis based on a 3-D high fidelity model of a realistic microwave imaging system for the clinical follow-up of brain stroke. The analysis is meant as a preliminary step towards the full experimental characterization of the system, with the aim of assessing the achievable results and highlight possible critical points. The system consists of an array of twenty-four printed monopole antennas, placed conformal to the upper part of the head; each monopole is immersed into a semi-solid dielectric brick with custom permittivity, acting as coupling medium. The whole system, including the antennas and their feeding mechanism, has been numerically modeled via a custom full-wave software based on the finite element method. The numerical model generates reliable electromagnetic operators and accurate antenna scattering parameters, which provide the input data for the implemented imaging algorithm. In particular, the numerical analysis assesses the capability of the device of reliably monitoring the evolution of hemorrhages and ischemias, considering the progression from a healthy state to an early-stage stroke.**

***Keywords*—Microwave imaging, numerical simulation, stroke, biomedical imaging, microwave antenna arrays, microwave propagation.**

I. Introduction

STROKE is a brain injury that occurs when oxygen-rich blood supply to the brain is interrupted, causing a severe damage in the affected area and leading to transitory or permanent disability or even death. It is triggered when a blood vessel of the brain either bursts (or ruptures) or is blocked by a clot. The first case, called intracranial hemorrhagic (ICH) stroke, is the most deadly, while the second one, called ischemic (IS) stroke, is the most common. Strokes represent a critical medical emergency and adequate and prompt diagnosis and treatment are essential to raise the probability of recovery and reducing the patients' damages, the risk of death, further disabilities, or a second onset [1], [2].

The incidence of stroke makes it the third-largest cause of death worldwide with over five millions of cases per year, and represents a genuine challenge for the ageing societies and the health system burden [3], [4]. Hence, industry, academic and medical communities have been working on technological solutions that improve the prognosis and support clinicians in the early diagnosis (identification, detection and localization) and subsequent treatment monitoring. Within the diagnosis support instruments, the most well-established imaging-based technologies are magnetic resonance imaging (MRI) and computerized X-ray tomography (CT) [5]. Although the mentioned technologies deliver highly reliable diagnostic information, there are intrinsic drawbacks in terms of portability, cost and safeness (for CT only) that limit their applicability.

These limitations have driven the development of novel complementary technologies for diagnostic imaging. Among the upcoming technologies, microwave imaging (MWI) is an enticing non-ionizing, low-intensity and cost-effective approach, which enables pre-hospital diagnosis of the kind of stroke, bedside brain imaging, and continuous monitoring during the post-acute stage. MWI relies on the contrast of the electrical properties (permittivity and conductivity) at microwave frequencies between healthy tissues of the brain and the stroke-affected ones (e.g., ischemic area versus regular gray or white matter).

In the last years, several researchers have been working on the development of MWI devices and prototypes for the detection, classification and monitoring of brain strokes, validating the promising capabilities of this technology. Currently, the most prominent industrial groups are Medfield Diagnostics AB with "Strokefinder", device used for the discrimination between ischemic and hemorrhagic strokes in the early stage, and EMTensor GmbH with "BrainScanner", a tomographic microwave brain scanner [6], [7]. Moreover, several prototypes have been realized by research groups in academia [8]–[12].

This paper deals with the microwave imaging prototype presented in [11] and presents the outcomes of a numerical analysis aimed at assessing its performance. In particular, the analysis is focused on the assessment of the capability of the device to perform the follow-up of either ischemic and hemorrhagic brain strokes, and it is meant as a preliminary step towards the full experimental characterization of the system, setting the achievable results and highlighting possible critical points. To this end, a 3-D high fidelity model based on a custom software is exploited. The accurate numerical modelling

Manuscript received XXX, 2020; accepted XXX. Date of publication XXX; date of current version XXX. This work was supported by the Italian Ministry of University and Research under the PRIN project "MiBraScan", and by the European Union's Horizon 2020 Research and Innovation Program under the EMERALD project, Marie Sklodowska-Curie grant agreement No. 764479. *(Corresponding author: Francesca Vipiana)*

D. O. Rodriguez-Duarte, J. A. Tobon Vasquez and F. Vipiana are with the Department of Electronics and Telecommunications, Politecnico di Torino, 10129 Torino, Italy (e-mail: francesca.vipiana@polito.it).

R. Scapaticci and L. Crocco are with the Institute for the Electromagnetic Sensing of the Environment, National Research Council of Italy, 80124 Naples, Italy (e-mail: scapaticci.r@irea.cnr.it; crocco.l@irea.cnr.it).

is essential to properly implement the imaging algorithm; in particular, it provides the device-specific electromagnetic (EM) operators required to build the imaging kernel, from whose accuracy depends the reliability and quality of the final outcome image. Moreover, a high fidelity numerical model allows to easily verify the capabilities of the realized MWI system, emulating the scattering parameters in input to the imaging algorithm, as well as virtually testing complex clinical scenarios and laboratory setups.

The paper is organized as follows. Section II covers the general description of the employed MWI system, the proposed EM modelling, and the implemented imaging algorithm. Then, Sect. III reports the obtained numerical results for the monitoring of the possible evolution of ICH and IS strokes, in either noiseless and noisy cases, with different levels of signal-to-noise-ratio (SNR). Finally, Sect. IV summarize the conclusions. Preliminary results have been reported in [13].

II. Materials and Methods

A. MWI System Requirements

The analyzed MWI system consists of an optimized 24-antenna-array distributed conformally to the upper part of the head (like a helmet), as shown in Fig. 1(a), where each antenna acts as transmitter and receiver. The number of antennas, their positions and orientation have been designed following the rigorous procedure proposed in [14], [15], that allows to keep low the system complexity while preserving imaging performance.

Each radiating element is composed by an optimized printed monopole and a brick-shaped semi-solid coupling medium as a single unit, locally tangent to the head surface [16]. The monopole is back fed by a rigid coaxial cable and immersed in the middle of the brick, as shown in Fig. 1(b)-(c), at 25 mm from the brick surface, which is flush with the head, to limit the near-field effects [17]. The working frequency band is chosen at around 1 GHz, while the coupling medium permittivity is $\epsilon_r \cong 20$ in order to have a good trade-off between the EM penetration inside the head tissues and the spatial imaging resolution. This choice is based on the multi-tissue analysis proposed in [18] where it is evident a "forbidden" band for the transmission coefficient between around 1.5 and 4 GHz.

B. EM Modelling

One crucial component to perform an accurate imaging reconstruction is the EM modeling of the whole MWI system. Reliable full-wave modeling provides accurate EM fields of the scenario under test and scattering parameters at the antenna ports. Here, we used a realistic 3-D CAD model working together with a full-wave software, based on the finite element method (FEM). The FEM solver employs the discretized volumes, defined on a tetrahedral mesh, of the whole CAD model with edge-basis functions, the curl-curl formulation for the electric field and Galerkin testing. The metal pieces, e.g. within the antenna, are stated as perfect electric conductor (PEC) surfaces and the dielectric sub-volumes, e.g. the bricks and the head, are modeled with the respective relative permittivity, ϵ_r, and conductivity, σ, associated to the corresponding tetrahedra. Lastly, the whole system is held in a discretized cylindrical container, terminated with absorbing boundary conditions (ABC) [19].

Regarding the antenna feeding, which is a crucial part to accurately compute the scattering parameters, each port is modeled as a section of a rigid coaxial cable, as shown Fig. 1(b). The metallic parts of the coaxial cable are modelled with PEC surfaces with no thickness and no tetrahedral mesh inside the metal, while its dielectric (lossless teflon) parts are discretized with tetrahedra with associated $\epsilon_r = 2.2$. The port section, S_p, where the tangential electric field is enforced when the antenna is excited, is at the end of the coaxial cable [green part in Fig. 1(b)]. On S_p proper boundary conditions are applied in order to emulate a matched coaxial cable [20], while above S_p a no-meshed PEC "cup" is placed to avoid a nonphysical coupling between the port section and the meshed parts outside the cable.

The scattering parameter for each pair of antenna ports, labelled as m and n, is then evaluated as

$$S_{mn} = \begin{cases} \frac{\iint_{S_p} \mathbf{E}_m \cdot \mathbf{E}_n^{\text{inc}}\, dS}{\iint_{S_p} |\mathbf{E}_n^{\text{inc}}|^2\, dS} & \text{if } m \neq n \\ \frac{\iint_{S_p} \mathbf{E}_n \cdot \mathbf{E}_n^{\text{inc}}\, dS}{\iint_{S_p} |\mathbf{E}_n^{\text{inc}}|^2\, dS} - 1 & \text{if } m = n \end{cases} \tag{1}$$

where $\mathbf{E}_n^{\text{inc}}$ is the electric field forced in the excited port n and $\mathbf{E}_m$ is the electric field evaluated at the port m via the FEM solver. $\mathbf{E}_n^{\text{inc}}$ can be represented with the transverse electromagnetic (TEM) mode of the coaxial cable as

$$\mathbf{E}_n^{\text{inc}} = \frac{V}{\sqrt{2\pi \ln(b/a)}} \frac{\hat{\rho}}{\rho}, \tag{2}$$

where a and b are the internal and external radii of the coaxial cable, and ρ and $\hat{\rho}$ are the radial coordinate and radial unit vector from the center of the coaxial cable in the port plane [20]. The coefficient V is chosen equal to 1 V.

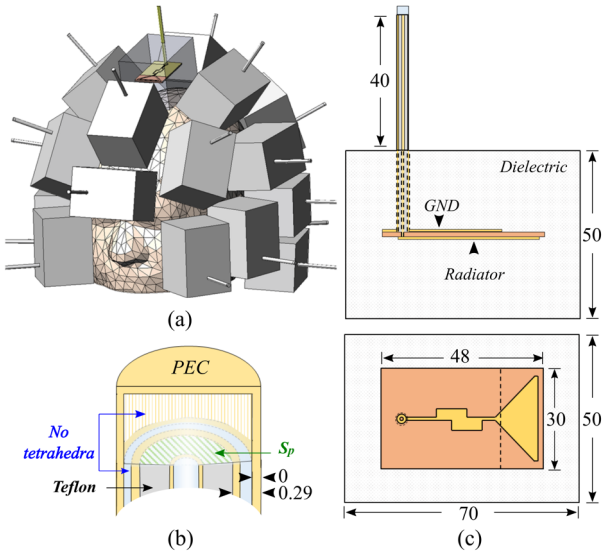

Fig. 1. Realistic geometrical models, units in mm; (a): conformal distribution of the antenna array around the head; (b): CAD model of the antenna feeding; (c): monopole antenna embedded into the dielectric brick.

The human head is modeled with the 3-D anthropomorphic phantom in [21], extracted from MRI data. Figure 2 shows the internal structure of the head phantom together with all the tissues included in the phantom and the values of their dielectric properties at 1 GHz [22]. This is considered as reference scenario of a healthy subject. Then, the stroke is modeled using a capsule-shaped container placed on back of the head, into the gray matter, as shown in Fig. 2. The capsule-shaped container can be fully or partially filled with a material mimicking dielectric properties of the hemorrhagic or ischemic stroke conditions [23], [24]. The monitoring will consider first the initial half-sphere (HS) stage and, then, its extension to the whole capsule (CAP).

C. Imaging Algorithm

Considering that the main application of the analyzed imaging system is the monitoring of the time evolution of the stroke and that the imaging targets are "small-concentrate" variations, a differential approach and the distorted Born approximation are adopted [25]. Under these assumptions, the mathematical framework of the underlying inverse scattering problem is simplified allowing real-time and reliable imaging of stroke's follow-up [26]. In details, the algorithm input is a differential scattering matrix, denoted as ΔS in the following, that takes into account the scattering matrices of the system in two distinct times. The output, say $\Delta\chi$, is a 3-D map of the electrical contrast variation in the respective period of time studied. $\Delta\chi$ is given by the ratio between the complex permittivity variation $\Delta\epsilon$, and the complex permittivity of the reference (unperturbed) state, denoted as ϵ_b. Then, by relying on the Born approximation, ΔS and $\Delta\chi$ are linearly related as

$$\Delta S_{p,q} = \mathcal{S}\left\{\Delta\chi\right\}, \tag{3}$$

where $\mathcal{S}$ is a linear and compact integral operator, whose kernel is $-j\omega\epsilon_b/(2\,a_p\,a_q)\,\mathbf{E}_{b,p}(\mathbf{r}_m)\cdot\mathbf{E}_{b,q}(\mathbf{r}_m)$, where the symbol "$\cdot$" denotes the dot product between vectors, $\omega = 2\pi f$ is the angular frequency, and a_p and a_q are the known incoming root-power waves at the p and q antenna ports respectively [27], [28]. $\mathbf{E}_{b,p}$ and $\mathbf{E}_{b,q}$ are the electric field radiated inside the imaging domain D at the reference state (i.e., unperturbed scenario) by the p and q antenna respectively, and $\mathbf{r}_m$ are the points in which the imaging domain D is sampled.

A reliable and well-established method to invert (3) is represented by the truncated singular value decomposition (TSVD) scheme [29], where the unknown differential contrast function is obtained through the inversion formula

$$\Delta\chi = \sum_{n=1}^{L_t} \frac{1}{\sigma_n}\,\langle \Delta S, u_n\rangle\, v_n, \tag{4}$$

where $\langle u, \sigma, v\rangle$ is the singular value decomposition (SVD) of the discretized scattering operator $\mathcal{S}$. L_t is the truncation index of the SVD, which acts as a regularization parameter, chosen such to meet a good trade off between stability and accuracy of the reconstruction [29].

III. Numerical Analysis Outcomes

The performed numerical analysis is meant to assess the performance of the modelled MWI system and its capability to monitor the time evolution of an hemorrhagic and ischemic stroke.

A. MWI System Setup

As mentioned in Sect. II-A, the modeled MWI has been designed to work at around 1 GHz. Then, to validate the adequate functioning as whole, including the head, the reflection and transmission coefficients of the antenna array are computed. The former, shown in Fig. 3, bears out the -10 dB frequency band from 800 MHz to 1.12 GHz for all antennas, in agreement with previous validations for a single antenna [16]. The variations among the different lines can be explained by different antenna orientations and different parts of the head close to the considered antenna. Moreover, Fig. 4 depicts the transmission coefficient for one of the lateral antennas with respect to the other 23 antennas, that is the base of the input differential matrices necessary for the imaging procedure. In all the frequency band and for all antenna pairs the amplitude of the transmission coefficient is above -90 dB, hence well above the noise floor of commercially available vector network analyzers (VNA).

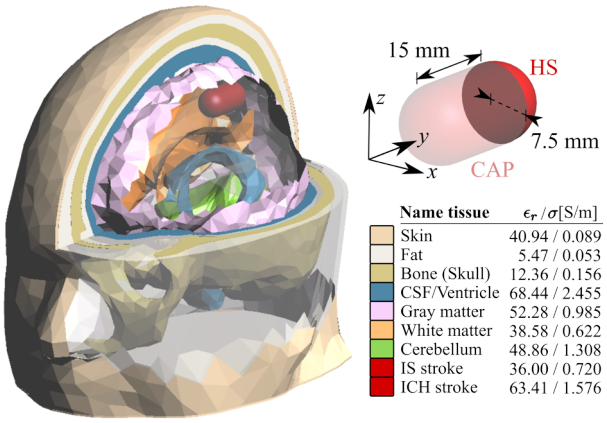

Fig. 2. (Left): multi-tissue head model; (top-right): half-sphere (HS) and capsule-shape (CAP) stroke models; (bottom-right): dielectric properties at 1 GHz of all the head tissues and hemorrhagic and ischemic strokes.

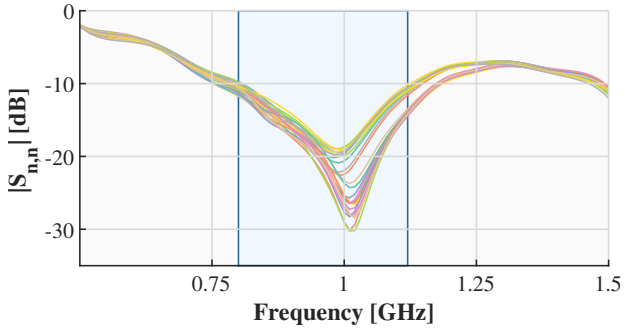

Fig. 3. Reflection coefficient amplitude; each line corresponds to the $|S_{n,n}|$ in dB for the n-th antenna of the MWI system with $n = 1, \ldots, 24$.

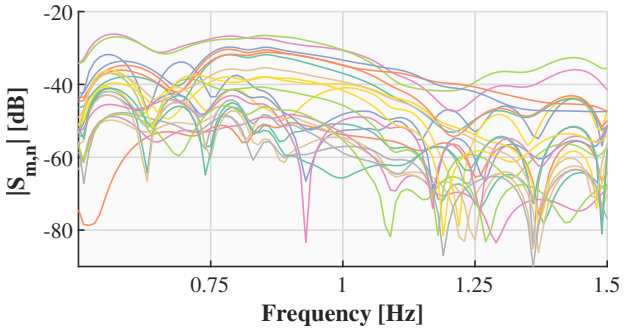

Fig. 4. Transmission coefficient amplitude; each line corresponds to the $|S_{m,n}|$ in dB with $n = 1$ (transmitting antenna) and $m = 2, \ldots, 24$ (receiving antennas).

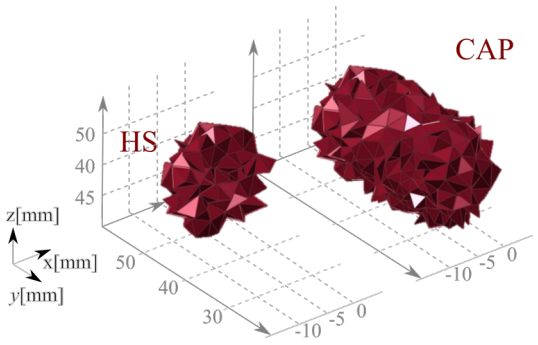

Fig. 5. Selection of tetrahedrons for ideal contrast; (left): HS case; (right): CAP case.

In the following, we consider two main stages of monitoring. The first stage covers the case when the patient evolves from a healthy condition to stroke. For this case, the scenario, at time instant t_0, is the healthy head and, at time instant t_1, is a stroke with a shape of a half-sphere with volume 0.88 cm^3 (see HS stroke in Fig. 2). We will refer to this case also as "detection phase". Instead, the second stage is indicated in the following as "post-onset monitoring": in this situation, at time instant t_0, the stroke has the half-sphere shape with volume 0.88 cm^3, while, at time instant t_1, its shape is extended to the whole capsule with volume 3.1 cm^3 (see CAP stroke in Fig. 2). Since the stroke dimensions and their growth depends on many factors, such as their location in the brain, the interested blood vessels and the time of their diagnosis [30]–[33], the dimensions and variations herein assumed are chosen such to show the ultimate potential of the proposed technology and they are related to the resolution of the MWI system at 1 GHz, that is around 1 cm.

To asses the performance of the discretized scattering operator $\mathcal{S}$, first of all, the "ideal" contrast of the monitoring cases described above is projected on its right singular vectors v_n that span the discretized contrast space. As ideal, we mean a contrast equal to 1 in the tetrahedrons where the stroke is present and equal to 0 anywhere else. Figure 5 shows the selected tetrahedrons when it is aimed the HS or the CAP case. The obtained projections, shown in Fig. 6, can be considered as the best possible reconstructions, for the two considered monitoring cases, with the modeled MWI system.

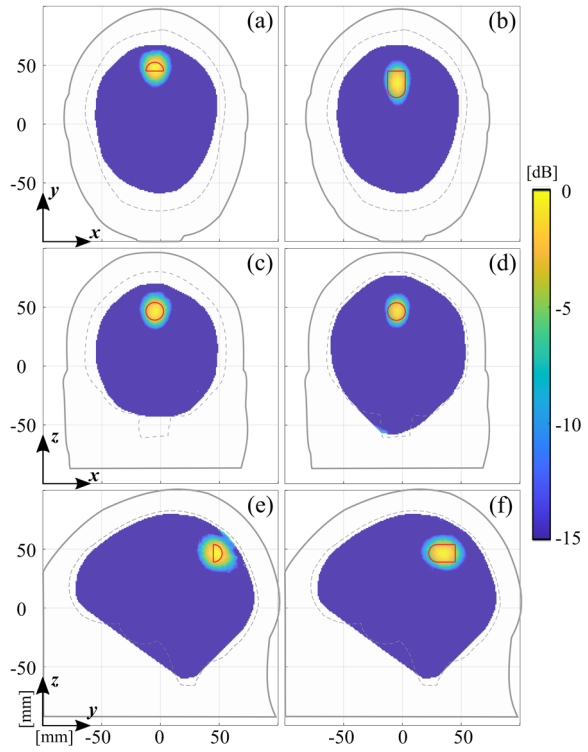

Fig. 6. Projection of the ideal dielectric contrast on the right singular vectors of the discretized scattering operator; the exact stroke location and shape are indicated by red contours. Left: HS case; right: CAP case. (a)-(b): transverse plane view; (c)-(d): frontal plane view; (e)-(f): sagittal plane view.

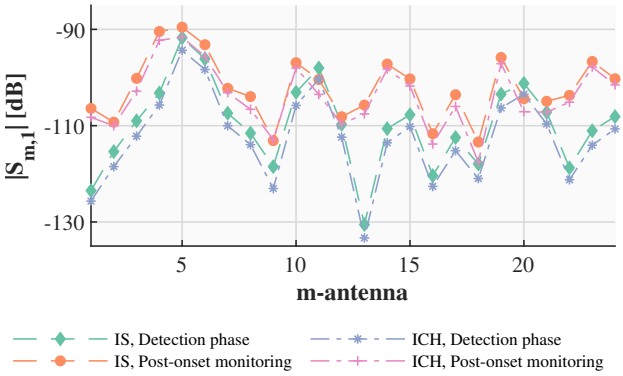

Fig. 7. Differential transmission coefficient amplitude of a lateral antenna with respect to the other antennas.

B. MWI Reconstructions

Here, we investigate the monitoring capabilities of the MWI system giving in input to the TSVD imaging algorithm the simulated differential scattering matrices. To highlight the level of the differential scattering parameters, in Fig. 7, the amplitude of the transmission coefficients of one antenna with respect to the others is reported. Two kind of strokes, ischemic and hemorrhagic, are considered together with the two monitoring cases previously described. In all cases, most of the differential coefficients are above -120 dB, hence within the dynamic range of a VNA with medium performance [34].

We can notice that the detection phase corresponds to lower transmission coefficients with respect to the post-onset

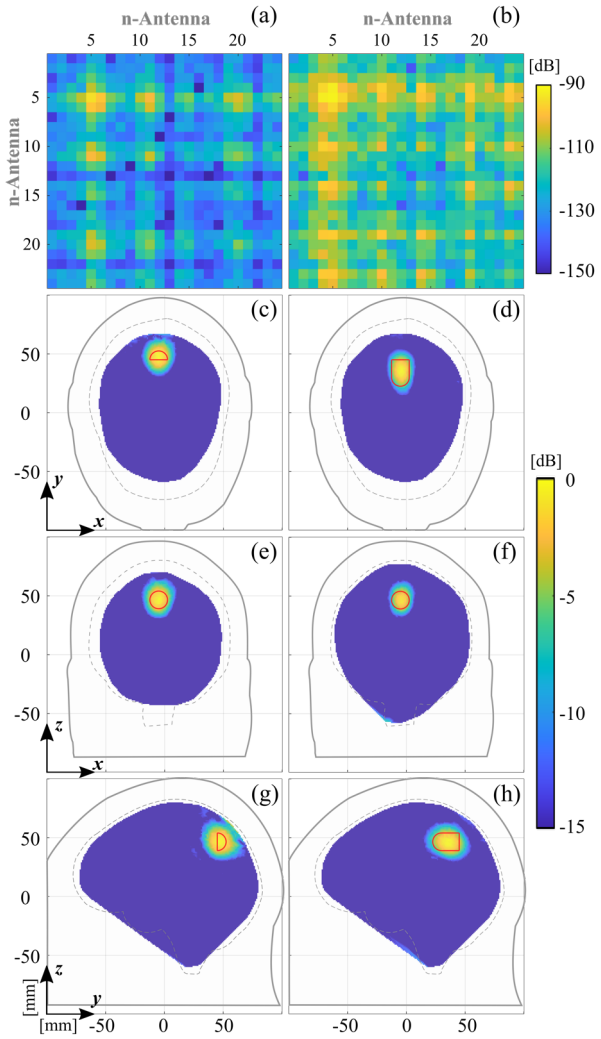

Fig. 8. Reconstructed images for a hemorrhagic stroke; the exact stroke location and shape are indicated by red contours. Left: detection phase; right: post-onset monitoring. (a)-(b): differential scattering matrices; (c)-(d):transverse plane view; (e)-(f): frontal plane view; (g)-(h): sagittal plane view.

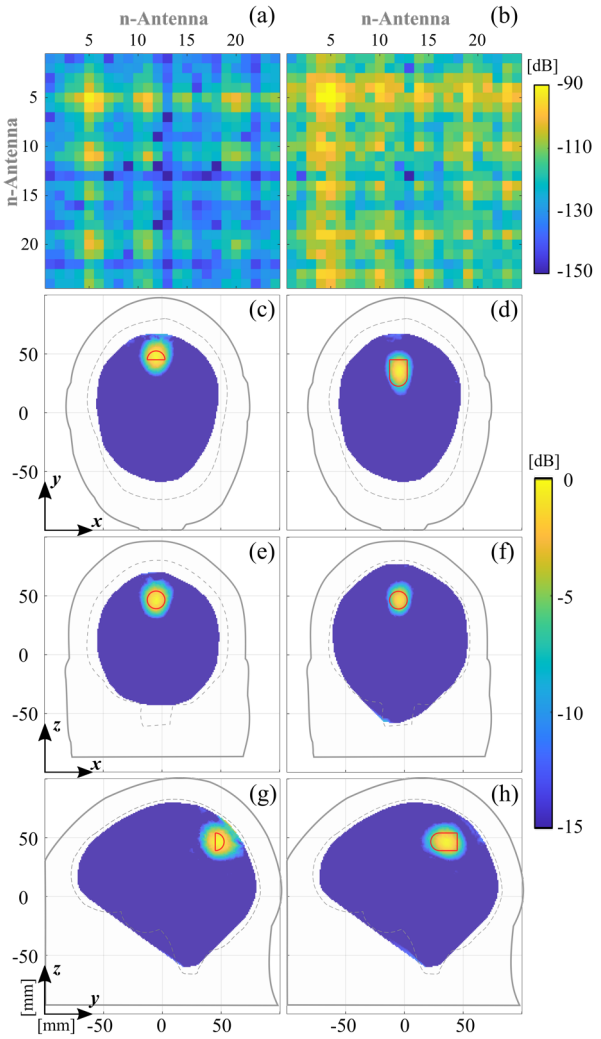

Fig. 9. Reconstructed images for a ischemic stroke; the exact stroke location and shape are indicated by red contours. Left: detection phase; right: post-onset monitoring. (a)-(b): differential scattering matrices; (c)-(d):transverse plane view; (e)-(f): frontal plane view; (g)-(h): sagittal plane view.

monitoring, where the stroke volume variation is larger.

In Fig. 8, the case of a hemorrhagic stroke is analyzed. The results in the first column correspond to the detection phase, instead the ones in the second column to the post-onset monitoring. The first row reports the differential scattering matrices and the following rows show the reconstructed images in the three main views. Good contrast reconstructions, almost identical to the corresponding projections shown in Fig. 5, are obtained in both cases, highlighting the progression of the stroke area from the initial half-sphere to the capsule-shape. Then, the same analysis is shown in Fig. 9 for the ischemic stroke.

Finally, Figs. 10 and 11 report the same cases considered in Figs. 8 and 9, respectively, adding noise to the scattering matrices. The synthetic data are corrupted by additive white Gaussian noise with two different levels assuming an input (source) power of 6 dBm: signal-to-noise ratio (SNR) equal to 100 dB for the results reported in the first columns and SNR equal to 90 dB for the ones in the second columns. The noise is added separately to the scattering matrices simulated at each time instant, which are then differentiated to obtain the noisy differential scattering matrices given in input to the imaging algorithm. We can see that in all the cases the expected contrast is well reconstructed even if the matrix pattern seems strongly affected by the added noise.

The shown reconstructions have been quantitatively evaluated via the root mean square error (RMSE) given by

$$\mathrm{RMSE} = \sqrt{\frac{\sum_{n=1}^{N_s} \left(\Delta\widehat{\chi} - \Delta\chi\right)^2}{N_s}}, \tag{5}$$

where N_s is the number of the samples of the discretized domain, $\Delta\widehat{\chi}$ the retrieved differential contrast (normalized to its maximum) and $\Delta\chi$ the actual normalized differential contrast. In Table I, we report the retrieved values of the RMSE for both hemorrhagic and ischemic strokes at all the considered levels of noise.

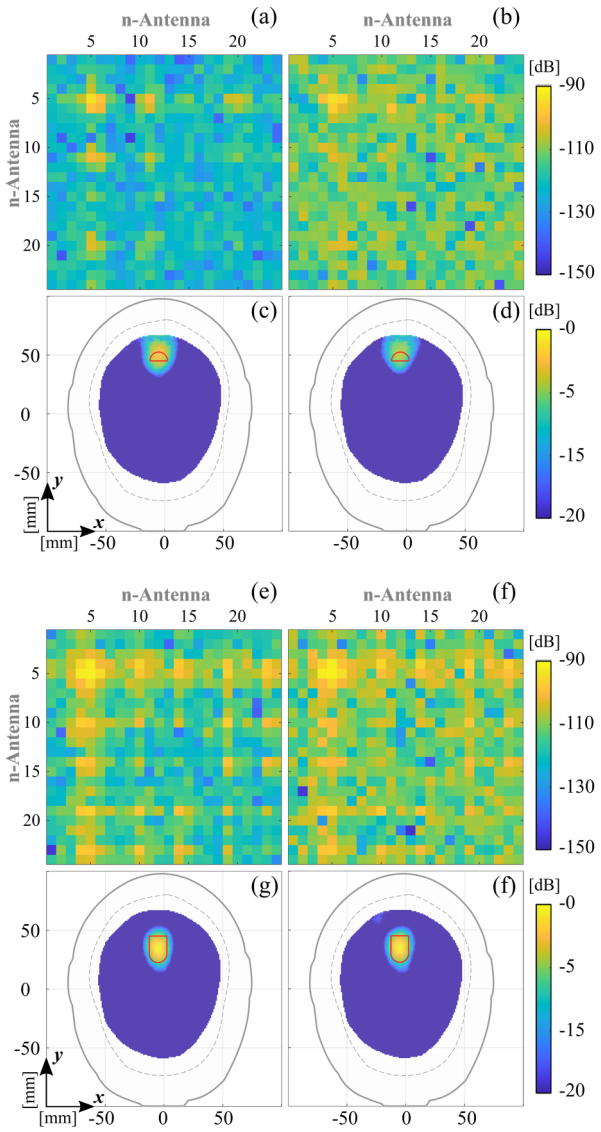

Fig. 10. Reconstructed images for a hemorrhagic stroke; the exact stroke location and shape are indicated by red contours. Left: SNR = 100 dB; right: SNR = 90 dB. (a)-(b): differential scattering matrices, detection phase; (c)-(d): reconstructed images in the transverse plane, detection phase; (e)-(f): differential scattering matrices, post-onset monitoring; (g)-(h): reconstructed images in the transverse plane, post-onset monitoring.

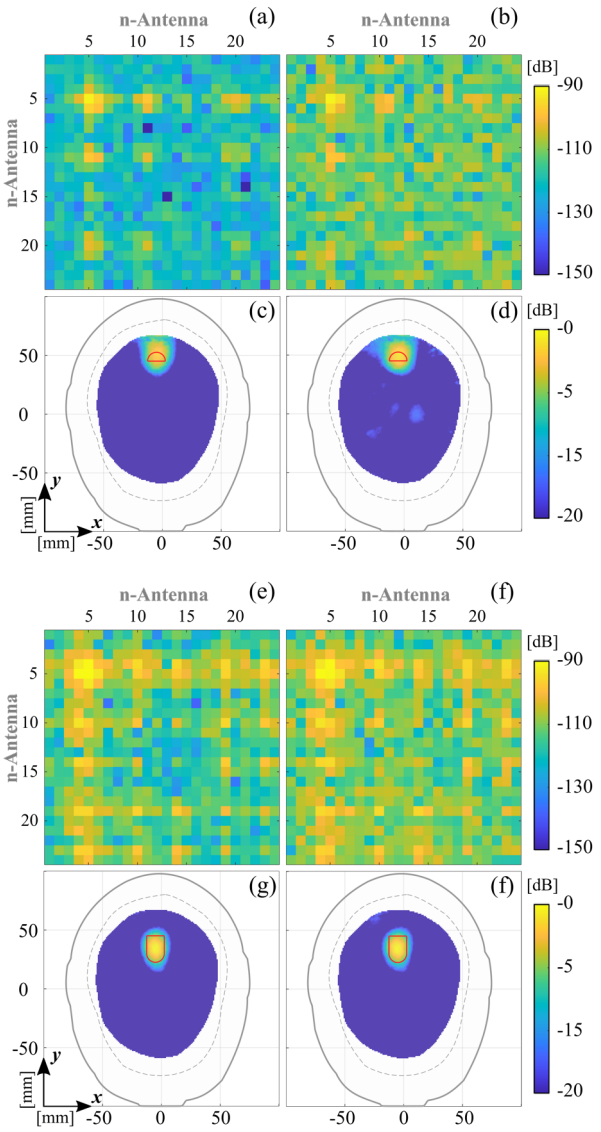

Fig. 11. Reconstructed images for a ischemic stroke; the exact stroke location and shape are indicated by red contours. Left: SNR = 100 dB; right: SNR = 90 dB. (a)-(b): differential scattering matrices, detection phase; (c)-(d): reconstructed images in the transverse plane, detection phase; (e)-(f): differential scattering matrices, post-onset monitoring; (g)-(h): reconstructed images in the transverse plane, post-onset monitoring.

TABLE I
RECONSTRUCTION RMSE

Stroke kind	SNR	Empty – HS	HS – CAP
Hemorrhagic	noiseless	0.078	0.112
	100 dB	0.079	0.123
	90 dB	0.103	0.130
Ischemic	noiseless	0.078	0.111
	100 dB	0.081	0.122
	90 dB	0.133	0.127

IV. CONCLUSION AND PERSPECTIVES

In this work the capabilities of a recently developed MWI prototype for the clinical follow-up brain stroke [11] have been assessed by means of a numerical analysis exploiting a custom 3-D high-fidelity numerical model of the system. The numerical analysis has shown that the system is indeed capable of performing the imaging of ischemic and hemorrhagic strokes with dimensions and/or variations of the order of 1 cm.

Given the overall reliability of the virtually performed assessment, the next step is to progress with actual experiments replicating the simulated scenarios so to achieve the final experimental assessment of the system. It is worth noting that, in so doing, the high-fidelity numerical model will still play a role as it will provide the device-specific mathematical operators needed to build in an accurate and reliable way the imaging kernel.

REFERENCES

[1] W. H. Organization, "The world health report 2002 - reducing risks, promoting healthy life." Available at http://www.who.int/whr/2002/en/.

[2] R. von Kummer, "Neuroimaging," in *Stroke Practical Guide for Clinicians* (N. Bornstein, ed.), pp. 64–74, Karger, 2008.

[3] T. Truelsen, B. Piechowski-Jozwiak, R. Bonita, C. Mathers, J. Bogousslavsky, and G. Boysen, "Stroke incidence and prevalence in Europe: a review of available data," *European Journal of Neurology*, vol. 13, no. 6, pp. 581–598, 2006.

[4] C. Johnson et al., "Global, regional, and national burden of stroke, 1990 – 2016: a systematic analysis for the global burden of disease study 2016," *The Lancet Neurology*, vol. 18, no. 5, pp. 439–458, 2019.

[5] K. B. Walsh, "Non-invasive sensor technology for prehospital stroke diagnosis: Current status and future directions," *Int. J. Stroke*, vol. 14, pp. 592–602, Jul. 2019.

[6] "EMTensor." Available at https://www.emtensor.com/.

[7] "Medfield." Available at https://www.medfielddiagnostics.com/en/.

[8] A. Fedeli, C. Estatico, M. Pastorino, and A. Randazzo, "Microwave detection of brain injuries by means of a hybrid imaging method," *IEEE Open Journal of Antennas and Propagation*, pp. 1–11, 2020.

[9] A. S. M. Alqadami, N. Nguyen-Trong, B. Mohammed, A. E. Stancombe, M. T. Heitzmann, and A. Abbosh, "Compact unidirectional conformal antenna based on flexible high-permittivity custom-made substrate for wearable wideband electromagnetic head imaging system," *IEEE Transactions on Antennas and Propagation*, vol. 68, pp. 183–194, Jan 2020.

[10] O. Karadima, M. Rahman, J. Sotiriou, N. Ghavami, P. Lu, S. Ahsan, and P. Kosmas, "Experimental validation of microwave tomography with the DBIM-TwIST algorithm for brain stroke detection and classification," *SENSORS*, vol. 20, Feb. 2020.

[11] J. A. Tobon Vasquez, R. Scapaticci, G. Turvani, G. Bellizzi, D. O. Rodriguez-Duarte, N. Joachimowicz, B. Duchene, E. Tedeschi, M. R. Casu, L. Crocco, and F. Vipiana, "A prototype microwave system for 3D brain stroke imaging," *SENSORS*, vol. 20, May 2020.

[12] J. A. Tobon Vasquez, R. Scapaticci, G. Turvani, G. Bellizzi, N. Joachimowicz, B. Duchêne, E. Tedeschi, M. R. Casu, L. Crocco, and F. Vipiana, "Design and experimental assessment of a 2D microwave imaging system for brain stroke monitoring," *Int. J. Antennas Propag.*, no. Article ID 8065036, p. 12 pages, 2019.

[13] D. Rodriguez-Duarte, J. A. Tobon Vasquez, and F. Vipiana, "Electromagnetic virtual prototyping of a realistic 3-D microwave scanner for brain stroke imaging," in *14th European Conference on Antennas and Propagation (EuCAP)*, March 2020.

[14] R. Scapaticci, J. Tobon, G. Bellizzi, F. Vipiana, and L. Crocco, "Design and numerical characterization of a low-complexity microwave device for brain stroke monitoring," *IEEE Transactions on Antennas and Propagation*, vol. 66, no. 12, pp. 7328–7338, 2018.

[15] R. Scapaticci, M. Bjelogrlic, J. A. Tobon Vasquez, F. Vipiana, M. Mattes, and L. Crocco, "Microwave technology for brain imaging and monitoring: Physical foundations, potential and limitations," in *Emerging Electromagnetic Technologies for Brain Diseases Diagnostics, Monitoring and Therapy* (L. Crocco, I. Karanasiou, M. James, and R. C. Conceicao, eds.), ch. 2, pp. 7–35, Springer int. pub., 2018.

[16] D. O. Rodriguez-Duarte, J. A. Tobon Vasquez, R. Scapaticci, L. Crocco, and F. Vipiana, "Brick shaped antenna module for microwave brain imaging systems," *IEEE Antennas and Wireless Propagation Letters*, pp. 1–5, 2020.

[17] O. M. Bucci, L. Crocco, R. Scapaticci, and G. Bellizzi, "On the design of phased arrays for medical applications," *Proc. IEEE*, vol. 104, pp. 633–648, Mar. 2016.

[18] R. Scapaticci, L. D. Donato, I. Catapano, and L. Crocco, "A feasibility study on Microwave Imaging for brain stroke monitoring," *Prog. Electromagn. Res. B*, vol. 40, pp. 305–324, 2012.

[19] E. A. Attardo, A. Borsic, G. Vecchi, and P. M. Meaney, "Whole-system electromagnetic modeling for microwave tomography," *IEEE Antennas Wirel. Propag. Lett.*, vol. 11, pp. 1618–1621, 2012.

[20] J. Jin and D. Riley, "Antenna source modeling and parameter calculation," in *Finite element analysis of antennas and arrays*, ch. 5, Hoboken, New Jersey: John Wiley and Sons Ltd, 1 ed., 2009.

[21] S. N. Makarov, G. M. Noetscher, J. Yanamadala, M. W. Piazza, S. Louie, A. Prokop, A. Nazarian, and A. Nummenmaa, "Virtual human models for electromagnetic studies and their applications," *IEEE Reviews in Biomedical Engineering*, vol. 10, pp. 95–121, 2017.

[22] D.Andreuccetti, R.Fossi, and C.Petrucci, "An internet resource for the calculation of the dielectric properties of body tissues in the frequency range 10 hz - 100 ghz. ifac-cnr, florence (italy), 1997. based on data published by c.gabriel et al. in 1996.." Accessed on: Feb. 28, 2020. [Online]. Available: http://niremf.ifac.cnr.it/tissprop/.

[23] S. Y. Semenov and D. R. Corfield, "Microwave tomography for brain imaging: feasibility assessment for stroke detection," *Int. J. of Antennas and Propagat.*, vol. 2008, p. 8 pages, 2008.

[24] D. Ireland and M. Bialkowski, "Feasibility study on microwave stroke detection using a realistic phantom and the FDTD method," in *2010 Asia-Pacific Microwave Conference*, pp. 1360–1363, 2010.

[25] R. Scapaticci, O. Bucci, I. Catapano, and L. Crocco, "Differential microwave imaging for brain stroke follow up," *Int. J. Antennas Propag.*, vol. 2014, no. Article ID 312528, pp. 1–11, 2014.

[26] I. Sarwar, G. Turvani, M. R. Casu, J. A. Tobon Vasquez, F. Vipiana, R. Scapaticci, and L. Crocco, "Low-cost low-power acceleration of a microwave imaging algorithm for brain stroke monitoring," *J. Low Power Electron.s Appl.*, vol. 8, no. 4, 2018.

[27] D. Tajik, F. Foroutan, D. S. Shumakov, A. D. Pitcher, and N. K. Nikolova, "Real-time microwave imaging of a compressed breast phantom with planar scanning," *IEEE Journal of Electromagnetics, RF, and Microwaves in Medicine and Biology*, vol. 2, no. 3, pp. 154–162, 2018.

[28] A. S. Beaverstone, D. S. Shumakov, and N. K. Nikolova, "Frequency-domain integral equations of scattering for complex scalar responses," *IEEE Transactions on Microwave Theory and Techniques*, vol. 65, no. 4, pp. 1120–1132, 2017.

[29] M. Bertero and P. Boccacci, *Introduction to Inverse Problems in Imaging*. Inst. Phys., Bristol, U.K., 1998.

[30] C. Laredo, Y. Zhao, S. Rudilosso, A. Renu, J. C. Pariente, A. Chamorro, and X. Urra, "Prognostic significance of infarct size and location: The case of insular stroke," *Scientific Reports*, vol. 8, pp. 1–10, 2018.

[31] A. Bruno, N. Shah, A. E. Akinwuntan, B. Close, and J. A. Switzer, "Stroke size correlates with functional outcome on the simplified modified rankin scale questionnaire," *Journal of Stroke and Cerebrovascular Diseases*, vol. 22, no. 6, pp. 781–783, 2013.

[32] J. L. Saver, "Time is brain-quantified," *Stroke*, vol. 37, no. 1, pp. 263–266, 2006.

[33] J. L. Saver, K. C. Johnston, D. Homer, R. Wityk, W. Koroshetz, L. L. Truskowski, and E. C. Haley, "Infarct volume as a surrogate or auxiliary outcome measure in ischemic stroke clinical trials," *Stroke*, vol. 30, no. 2, pp. 293–298, 1999.

[34] Keysight Technologies, "Keysight streamline series USB vector network analyzer P937XA 2-port, up to 26.5 GHz," *Data Sheet*, Oct. 2018.

David O. Rodriguez-Duarte received the B.Sc. and M.Sc. degrees in electronic engineering from Universidad Nacional de Colombia, Bogota, Colombia, in 2013 and 2018. He works toward the PhD degree with the Department of Electronics and Telecommunications at Politecnico di Torino (Italy), with the applied electromagnetics group. He is currently a Marie Sklodowska-Curie Fellow involved in the modelling and designing microwave imaging systems for cerebrovascular diseases as part of the European project EMERALD. From 2014 to 2015, he collaborated in satellite mission Libertad 2 as a Young Researcher with the Control and Energy Nanosatellites group, Universidad Sergio Arboleda, Bogota, Colombia. In 2017, he was visitor research at the University of British Columbia, Kelowna, BC, Canada, working on Unmanned Aerial Vehicle for information collection/dissemination in Wireless Sensor Networks funding by the Emerging Leaders in the Americas Program. His current research interest includes antenna design and microwave imaging system for medical applications.

Jorge A. Tobón Vasquez received a Ph.D. Degree in Electronics and Telecommunication Engineering from the Politecnico di Torino, Italy, in 2014. He completed the Master's Degree in Electronic Engineering at the Politecnico di Torino and the Degree in Electronics Engineering at the Universidad de Antioquia, Colombia, both in 2010, as part of a double degree agreement. In 2010 he collaborated with the Antennas and Electromagnetic Lab (LACE), Istituto Superiore Mario Boella (ITA). In 2014 worked as a researcher at Istituto Superiore Mario Boella. He works now at Politecnico di Torino: from 2015 until 2018 as a post-doc researcher, and since 2019 as Assistant Professor. His main research activities correspond to the development of numerical techniques applied on the integral equations, based on domain decomposition; the study and modeling of electromagnetic propagation in non-homogeneous media, in particular, the analysis of radio communication between spatial re-entry vehicles and the ground stations; and modeling, designing, and analyzing systems for microwave imaging applications, specifically in the biomedical and food industry fields. In 2018 received the "Premio Latmiral," an award granted by the Italian Society of Electromagnetism (SIEm). In 2020 he received the URSI General Assembly & Scientific Symposium (GASS) Young Scientist Award (YSA) and the URSI National Meeting Young Scientist Paper Award (named after prof. Sorrentino). During his research activities, he has worked on different projects like National Italian research projects MICENEA and MIBRASCAN, and Innovative Training Network (MSCA) EMERALD.

Rosa Scapaticci was born in Naples, Italy, in 1985. She received the Laurea degree (summa cum laude) in biomedical engineering from "Federico II" University of Naples, Naples, Italy, in 2010 and the Ph.D. degree in Information Engineering from "Mediterranea" University of Reggio Calabria, Reggio Calabria, Italy, in 2014. From December 2013 she has been working at the Institute of Electromagnetic Sensing of the Environment, National Research Council of Italy (IREA-CNR), Naples, Italy, first as a Research Fellow and from September 2017 as a Researcher. She is co-author of more than 60 papers on international journals and conference proceedings. In 2013, she received the best Student Member Paper Award from the IEEE Antennas and Propagation Society Central and Southern Italy Chapter. She received from the Italian Society of Electromagnetics, the Barzilai Award and the Latmiral Award in September 2014 and in September 2018, respectively. Her scientific interests include electromagnetic scattering problems, imaging methods for noninvasive diagnostics and they are mainly focused on the development of innovative microwave imaging approaches in the framework of biomedical applications, as well as therapeutic applications of electromagnetic fields.

Lorenzo Crocco is a Research Director with the Institute for the Electromagnetic Sensing of the Environment, National Research Council of Italy (IREA-CNR). His scientific activities mainly concern electromagnetic scattering, with a focus on diagnostic and therapeutic uses of EM fields, through-the-wall radar and GPR. On these topics, he has published more than 120 papers, given keynote talks and led or participated to research projects. He is associate editor for the IEEE Journal of Electromagnetics, RF and Microwaves in Medicine and Biology (IEEE J-ERM) and has edited a book on Electromagnetic Technologies for Brain Diseases Diagnostics, Monitoring and Therapy. From 2013 he is Italian representative in the Management Committees of COST actions devoted to medical applications of EM fields (MiMed on microwave imaging and MyWAVE on therapeutic applications of electromagnetic waves). Since 2017, he is Member of the Board of Directors of the Italian Electromagnetic Society (SIEm). In 2018, he received the full professor habilitation in electromagnetic fields, by the Italian Ministry of Research and University. Since 2019, he is a member of the Italian URSI Commission. In 2019, he has been elected in the Scientific Board of the Engineering Department (DIITET) of CNR. Dr. Crocco has been the recipient of the SIEm "Barzilai" Award for Young Scientists (2004) and YSA at the URSI General Assembly held in New Delhi (India) in 2005.

Francesca Vipiana (M'07–SM'13) received the Laurea and Ph.D. (Dottorato di Ricerca) degrees in electronic engineering from the Politecnico di Torino, Torino, Italy, in 2000 and 2004, respectively, with doctoral research carried out partly at the European Space Research Technology Center, Noordwijk, The Netherlands.

From 2005 to 2008, she was a Research Fellow with the Department of Electronics, Politecnico di Torino. From 2009 to 2012, she was the Head of the Antenna and EMC Lab with the Istituto Superiore Mario Boella, Torino. Since 2012, she has been an Assistant Professor with the Department of Electronics and Telecommunications, Politecnico di Torino, where she has been an Associate Professor since 2014. Her current research interests include numerical techniques based on the integral equation and method of moment approaches, with a focus on multiresolution and hierarchical schemes, domain decomposition, preconditioning and fast solution methods, Green's function regularization, and advanced quadrature integration schemes. She is involved in the analysis, synthesis, and optimization of multiband reconfigurable compact antennas, and in the modeling and design of microwave imaging systems for medical and industrial applications.

Prof. Vipiana received the Lot Shafai Mid-Career Distinguished Award from the IEEE Antennas and Propagation Society in 2017, and she is currently in the Editorial Board of the IEEE Transactions on Antennas and Propagation and of the IEEE Antennas and Propagation Magazine.